Nuclear Medicine & Biology, Vol. 27, pp. 661–670, 2000

ISSN 0969-8051/00/$–see front matter
PII S0969-8051(00)00137-2

Graphical Analysis of PET Data Applied to Reversible and Irreversible Tracers

Jean Logan

CHEMISTRY DEPARTMENT, BROOKHAVEN NATIONAL LABORATORY, UPTON, NEW YORK, USA

ABSTRACT. The differential equations of compartmental analysis form the basis of the models describing the uptake of tracers used in imaging studies. Graphical analyses convert the model equations into linear plots, the slopes of which represent measures of tracer binding. The graphical methods are not dependent upon a particular model structure but the slopes can be related to combinations of the model parameters if a model structure is assumed. The input required is uptake data from a region of interest vs time and an input function that can either be plasma measurements or uptake data from a suitable reference region. Graphical methods can be applied to both reversible and irreversibly binding tracers. They provide considerable ease of computation compared to the optimization of individual model parameters in the solution of the differential equations generally used to describe the binding of tracers. Conditions under which the graphical techniques are applicable and some problems encountered in separating tracer delivery and binding are considered. Also the effect of noise can introduce a bias in the distribution volume which is the slope of the graphical analysis of reversible tracers. Smoothing techniques may minimize this problem and retain the model independence. In any case graphical techniques can provide insight into the binding kinetics of tracers in a visual way. NUCL MED BIOL 27;7:661–670, 2000. **© 2000 Elsevier Science Inc. All rights reserved.**

KEY WORDS. Graphical analysis, Compartmental modeling, Distribution volume, Influx constant

INTRODUCTION

Graphical analysis refers to the transformation of multiple time measurements of plasma and tissue uptake data into a linear plot, the slope of which is related to the number of available tracer binding sites. This type of analysis allows easy comparisons among experiments. No particular model structure is assumed which can be an advantage in many cases since one model may not describe equally well all data sets from the same region of interest (ROI). It is assumed that the plasma concentrations of unchanged tracer are monitored following tracer injection. The requirement of plasma measurements can be eliminated in some cases when a reference region is available. There are two categories of graphical methods that apply to two general types of ligands—those that bind reversibly during the scanning procedure (14) and those that are irreversible or trapped during the time of the scanning procedure (1, 11, 20, 21, 25, 26). This distinction between reversible and irreversible depends on the length of the experiment. A ligand might be reversible over a period of many hours or days, but for the hour or so of the experiment it could be considered irreversible. It is not always possible to distinguish reversible from irreversible tracers from uptake data alone.

Graphical analysis techniques have been applied extensively to tracers used in neuroreceptor imaging, but their application is not limited to these studies. The examples presented here are taken from receptor studies in the brain, but the problems illustrated will be relevant to other applications.

Address correspondence to: Jean Logan, Brookhaven National Laboratory, Chemistry Department, Upton, NY 11973, USA; E-mail: jlogan@bnl.gov.

GRAPHICAL ANALYSIS OF REVERSIBLE LIGANDS

For reversible systems the form of the graphical analysis equation can be derived from the compartmental equations describing tracer accumulation in tissue (14, 21). For the two-tissue compartment model shown below the compartment equations are given in Eq. (1):

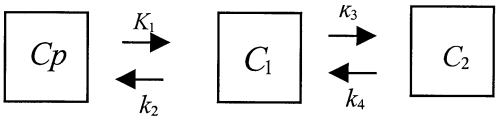

$$\frac{dC_1}{dt} = K_1 Cp(t) - (k_2 + k_3)C_1 + k_4 C_2$$
$$\frac{dC_2}{dt} = k_3 C_1 - k_4 C_2 \qquad (1)$$

where C_1 and C_2 are concentrations (or radioactivities) for each compartment at time t. The units of radioactivity used in the examples presented in this paper are nCi/mL. The transfer constants k_2, k_3, and k_4, respectively, describe the efflux from tissue to plasma; the specific binding of tracer to a receptor, transporter, or enzyme; and the dissociation from that specific binding. The units of these constants throughout this paper are min^{-1}. k_3 is the product of a bimolecular rate constant ($pmol^{-1}$ min^{-1}) and the concentration of free receptor/enzyme (pmol) which is assumed to be constant, although in experiments with changing neurotransmitter levels it represents an average over the experiment. K_1, which is expressed in units of mL min^{-1} mL^{-1}, describes transfer from plasma to tissue and is a function of blood flow, capillary permeability, and plasma protein binding. Cp is the plasma concentration (nCi/mL) of the unchanged tracer. Using ROI(t) = C_1 + C_2 + $VpCp$, that is, the sum of radioactivities from all compartments in

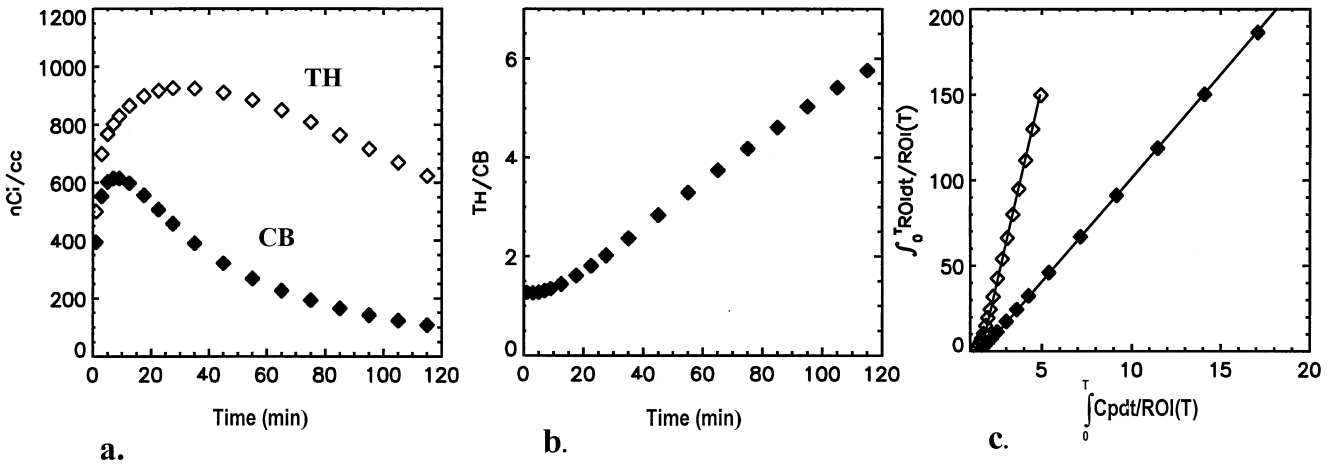

FIG. 1. (a) Simulated data; upper curve (TH) has a DV = 45 mL mL^{-1}, lower curve (CB) DV = 12 mL mL^{-1}. (b) Ratio of uptake TH/CB. (c) Graphical analysis of data in (a).

a given region of interest plus a contribution from the regional blood volume Vp, Eq. (1) can be rearranged into Eq. (2):

$$\frac{\int_0^t \mathrm{ROI}(t')\,dt'}{\mathrm{ROI}(t)} = \left[\frac{K_1}{k_2}\left(1+\frac{k_3}{k_4}\right)+Vp\right]\frac{\int_0^t Cp(t')\,dt}{\mathrm{ROI}(t)} + int \quad (2)$$

which is a linear form when the second term (int) on the right-hand side of Eq. (2) is constant. The individual points are defined by the scanning times t. The term int for the two-compartment model is given by (neglecting Vp) Eq. (3):

$$-\frac{1}{k_2}\left[1+\frac{k_3}{k_4}\right]-\frac{C_2(t)}{k_4[C_1(t)+C_2(t)]} \quad (3)$$

A plot of $\int_0^t \mathrm{ROI}(t')\,dt'/\mathrm{ROI}(t)$ versus $\int_0^t Cp(t')\,dt'/\mathrm{ROI}(t)$ for times t is linear after some time t^*. The slope is the total tissue distribution volume (DV) plus the plasma contribution. DV is related to the number of unoccupied binding sites through k_3 and is expressed in units of mL mL^{-1} (3). For a one-compartment model DV is K_1/k_2, the ratio of transport constants. Although the effects of blood flow, capillary permeability, and plasma protein binding are implicitly included in K_1 and k_2, their ratio is not a function of blood flow (15). Nonspecific binding is also included in k_2 (3).

The condition for linearity of Eq. (2) is that the intercept (int) is constant. For some time $t > t'$, the compartment concentrations follow the plasma concentration so that $(C_1 + C_2) \propto Cp$ and $C_2 \propto Cp$ (the steady-state condition), which ensures that int is constant since Cp cancels. In many cases the intercept becomes constant even before $(C_1 + C_2)/Cp$ becomes constant so that the graphical method can be applied before the steady-state condition becomes valid, that is, for some time $t^* < t'$. Consider the example (simulated data) in Figure 1. ROIs with DVs of 45 thalamus (TH) and 12 cerebellum (CB) (mL mL^{-1}) are illustrated. Figure 1b illustrates the ratio of uptake for these two ROIs (TH/CB). The increasing ratio indicates that the steady-state condition has not been reached, at least not for the higher DV region. However, the graphical analysis (Fig. 1c) is linear and gives the correct DV for both ROIs. To understand why this occurs, consider the time dependence of $(C_1 + C_2)/Cp$ compared to that of the intercept for the two-tissue compartment model [contained in $C_2/(C_1 + C_2)$ in Eq. (3)]. The limiting value of the time-dependent portion of the intercept is given by $C_2(t)/C_1(t) + C_2(t) \rightarrow 1/1 + k_4/k_3$. From Table 1, the tissue-to-plasma ratio varies by more than 40% for times from 35 min to 115 min, while the ratio $C_2/(C_1 + C_2)$ varies only by about 5% and is effectively constant at 35 to 40 min. Thus the steady-state condition is not a requirement for the graphical method to be valid. The intercepts from the graphical analysis for one- and two-compartment models are $-1/k_2$ and $-\{(1/k_2)(1 + k_3/k_4) + 1/[k_4(1 + k_4/k_3)]\}$, respectively. Estimates of K_1 can be made by taking the ratio of the slope to $(-)$ the intercept. This will be valid for the two-compartment model when the second term in the intercept is small compared to the first.

TABLE 1. Comparison of the Ratio of Compartment Concentrations* versus Time for the Data Shown in Figure 1a (◇)

Time	$C_2/(C_1 + C_2)$	$(C_1 + C_2)/Cp$
35	0.72	52
45	0.726	58
55	0.73	64
65	0.75	71
75	0.752	77
85	0.756	83
105	0.76	87
115	0.76	91

* Specifically bound compartment (C_2) to total ($C_1 + C_2$).

Figure 2 illustrates simulated data with the same DV but with very different kinetics. For the upper curve (Fig. 2a), the main contribution to the DV is from the ratio of transport constants $\lambda = K_1/k_2$, while for the lower curve the main contribution is from the ratio of binding constants. The graphical analysis is illustrated in Figure 2b. Both achieve linearity but with very different times t^*, which will affect the length of scanning time required to obtain an accurate estimate of the DV. Since the graphical analysis depends upon the integral of the tissue activity, it is not possible to eliminate the early scans.

The distribution volume, which is related to the number of tracer binding sites, has been found to be estimated with much higher accuracy than individual model parameters (3). Furthermore, comparisons between DVs obtained from a nonlinear least squares

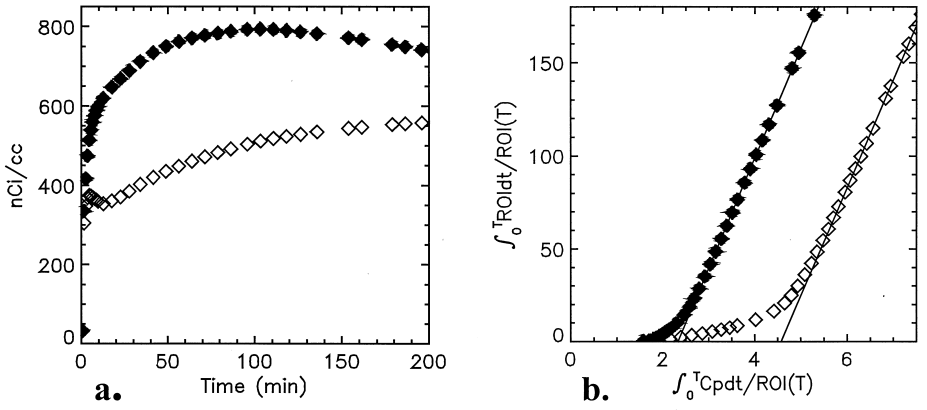

FIG. 2. (a) Both curves (simulated data) have the same DV but very different kinetics. The model parameters are given. (b) Graphical analysis of the data in (a) indicating a difference in t^*, the initial time at which the analysis becomes linear.

	λ	K_1	k_3	k_4	k_3/k_4	DV	
	(mL/mL)	mL min^{-1}/mL	min^{-1}	min^{-1}		(mL/mL)	
◇	**3.0**	**.6**	**.1**	**.005**	**20**	**60**	**t*=80**
◆	**10.**	**.5**	**.1**	**.02**	**5.0**	**60**	**t*=35**

(NLLSQ) fit to a particular model and the DVs determined graphically have been found to be in good agreement, for example data from [^{11}C]raclopride positron emission tomography (PET) studies in humans using ROI analysis (13). Koeppe *et al.* compared the graphical analysis to compartmental analysis for (+)-α-[^{11}C]-dihydrotetrabenazine (DTBZ), which binds to the vesicular monoamine transporter, finding agreement within 5% for ROI data (13). They also found that images constructed using the graphical method and the weighted integral method were essentially equivalent.

The total distribution volume contains within it effects of plasma protein binding (K_1) and nonspecific binding (15). The kinetic constants for nonspecific binding are assumed to be sufficiently rapid that it is always in a steady state (19) and is implicitly included in model parameters. For example, the model parameter k_3 is actually $f_{NS}\,k_3'$ where f_{NS} is the free fraction of tracer in tissue (*NS* refers to the ratio of binding constants for nonspecific binding). By taking the ratio of the DV from an ROI with a significant number of binding sites to that of a reference region (devoid of binding sites) we have the distribution volume ratio (DVR) given by Eq. (4):

$$\mathrm{DVR} = \frac{\dfrac{K_1}{k_2}\left(1 + \dfrac{k_3}{k_4}\right)}{K_1^{ref}/k_2^{ref}} = 1 + \frac{k_3}{k_4} \tag{4}$$

if the ratio of transport constants (K_1/k_2) is the same in both regions. In this case the dependence upon plasma protein binding is removed, since $K_1/k_2 \propto 1/fp$, where fp is the tracer fraction not bound to plasma proteins (3). The DVR is expressed in terms of the ratio of binding constants (k_3/k_4), which is related to the binding potential (19) but contains the effects of nonspecific binding. Clearly it is important that the DVR be sufficiently greater than 1 so that it will contain information about tracer binding sites. We have found reproducibility on test/retest is improved when the DVR is used for comparison rather than the DV (23). It may be that the effects of plasma protein binding are more variable than that of nonspecific binding, and this contributes to improved reproducibility. Also the ratio would tend to cancel errors in the metabolite correction to the plasma input function between experiments.

The DV and DVR have been used in many experiments in which neurotransmitter levels are manipulated through pharmacological intervention [for example (4)]. Although the free receptor concentration is most likely not constant but changing in response to the neurotransmitter pulse (or dip), the data can still be analyzed in terms of the DV (or DVR) where the DV now represents an average over the course of the experiment. Endres and Carson (6) have performed simulations showing how the kinetic properties of tracers determine the magnitude of change in the DV due to a variation in neurotransmitter concentration.

DISTRIBUTION VOLUME RATIOS USING A REFERENCE REGION (WITHOUT BLOOD SAMPLING)

The DVR can be calculated directly with the graphical method by using data from a reference region [REF(t)] with an average tissue-to-plasma efflux constant, $\bar{k}_2$ (to approximate the plasma integral) (17) [see Eq. (5)]:

$$\frac{\displaystyle\int_0^T \mathrm{REF}(t)\,dt}{\mathrm{REF}(T)} = \lambda\,\frac{\displaystyle\int_0^T Cp(t)\,dt}{\mathrm{REF}(T)} - \frac{1}{k_2^{\mathrm{REF}}} \quad \text{where} \quad \lambda = K_1^{\mathrm{REF}}/k_2^{\mathrm{REF}} \tag{5}$$

Solving for $\int_0^T Cp\,dt$ and substituting in Eq. (2), replacing k_2^{REF} with $\bar{k}_2^{\mathrm{REF}}$, gives Eq. (6):

$$\frac{\displaystyle\int_0^T \mathrm{ROI}(t)\,dt}{\mathrm{ROI}(t)} = \mathrm{DVR}\left[\frac{\displaystyle\int_0^T \mathrm{REF}(t)\,dt + \mathrm{REF}(T)/\bar{k}_2^{\mathrm{REF}}}{\mathrm{ROI}(T)}\right] + int' \tag{6}$$

where int' is $int + \delta$, δ is the error term given by Eq. (7):

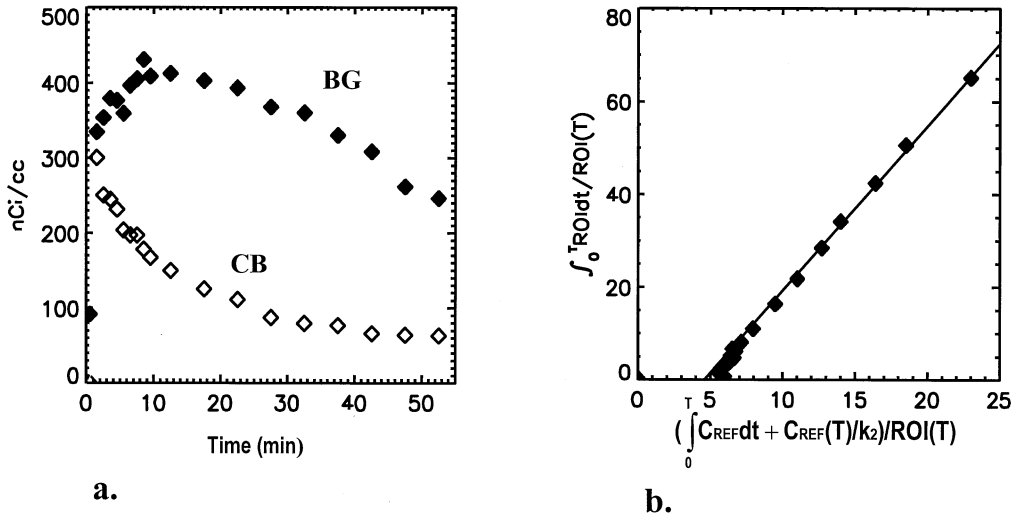

FIG. 3. (a) PET study with [^{11}C]raclopride. The upper curve is an ROI from the basal ganglia (BG) and the lower curve is a reference region from the cerebellum (CB). (b) Graphical analysis using CB as the reference region, $\bar{k}_2 = 0.16$ min^{-1}, DVR = 3.52 mL mL^{-1} ($r = 0.999$, sum of squares of residuals 4.5).

$$\delta = \mathrm{DVR}\left(\frac{1}{k_2^{\mathrm{REF}}} - \frac{1}{\bar{k}_2^{\mathrm{REF}}}\right)\frac{\mathrm{REF}(T)}{\mathrm{ROI}(T)} \qquad (7)$$

TABLE 2. Comparison of the DVs Computed Graphically (GR) and by the NLLSQ Methods for the ROIs BG (◆) and CB (◇) (Fig. 3a) for [^{11}C]Raclopride

	DV_{GR}	DV_{NLLSQ}
BG	1.72	1.70
CB	0.484	0.437[a]
DVR_{GR}	3.55	
DVR_{NLLSQ}	3.86	
DVR_{REF}	3.52	

The DVR for both GR and NLLSQ methods are compared with the DVR from a reference region (CB).

[a] NLLSQ underestimates radioactivity in CB with a one-compartment model.

(DVR = DV/λ).

When $(\mathrm{DVR}/k_2)\mathrm{REF}(T)/\mathrm{ROI}(T)$ is small and/or reasonably constant, the term containing k_2^{REF} in Eq. (6) can be neglected. Figure 3 illustrates use of a reference region for [^{11}C] raclopride ($\bar{k}_2 = 0.16$ min^{-1}). The upper curve is from an ROI in the basal ganglia that contains specific binding sites. The lower curve is from the cerebellum, which does not contain specific binding sites. There is essentially no difference between the DVR calculated with $\bar{k}_2 = 16$ min^{-1} and with $\bar{k}_2 = \infty$ (DVR = 3.53). Comparing the reference DVR to that calculated from parameters determined from an NLLSQ method (Table 2), we find the DVR greater for the NLLSQ method due to the fact that the reference region has a lower DV than that found by the graphical method. This is because for this subject the one-compartment model for the reference region (CB) underestimates the DV.

Another example of the DVR calculated from a reference region is taken from a study with the dopamine transporter tracer [^{11}C]-*d-threo*-methylphenidate (24) (Fig. 4), which has a smaller value of k_2 than

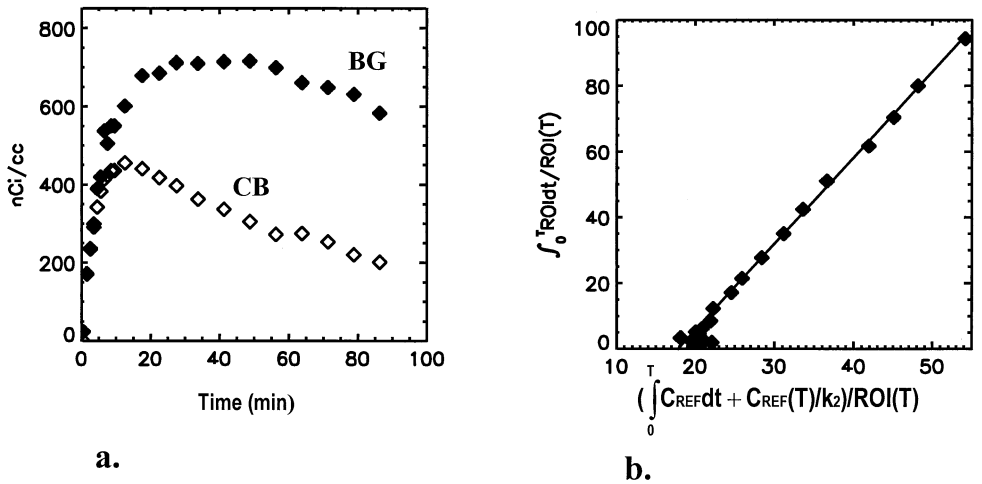

FIG. 4. (a) PET study with [^{11}C]*d-threo*-methylphenidate; BG (◆) and CB (◇). (b) Graphical analysis using a reference region $\bar{k}_2 = 0.05$ min^{-1}, DVR = 2.59 mL mL^{-1} ($r = 0.998$, sum of squares of residuals 7.4).

TABLE 3. Comparison of the DVs Computed Graphically (GR) and by the NLLSQ Methods for the ROIs BG (◆) and CB (◇) (Figure 3a) for [^{11}C]d-*threo*-Methylphenidate

	DV_{GR}	DV_{NLLSQ}
BG	27.7	27.9
CB	10.2	10.04
DVR_{GR}	2.72	
DVR_{NLLSQ}	2.78	
DVR_{REF}	2.59	

	Variation in DVR with k_2	
	k_2	DVR
	0.03	2.78
"True" k_2	0.04	2.70
Average k_2	0.05	2.59
Without k_2		2.32

The DVR for both GR and NLLSQ methods are compared with the DVR from a reference region (CB) using an average k_2 ($\bar{k}_2$). The variation of DVR_{REF} with k_2 is also shown.

raclopride. The DVR for methylphenidate is much more sensitive to the value used for $\bar{k}_2^{REF}$. From Table 3 with $\bar{k}_2 = \infty$, the DVR is 15% less than that calculated by using blood data. Using the average value of k_2, the DVR is only 5% less. For comparison the graphical and NLLSQ methods using the plasma input function give equivalent results but somewhat higher than the reference method.

Ichise has proposed an alternative to Eq. (6), which is a multilinear regression (12). This method appears to provide the same results as Eq. (6) with $k_2^{REF} = \infty$ (16).

GRAPHICAL ANALYSIS OF IRREVERSIBLE LIGANDS

Irreversibly binding ligands are essentially trapped for the time course of the scanning procedure. In terms of the two-compartment model pictured above, $k_4 = 0$ so that tracer in C_2 is trapped. Patlak *et al.* (20, 21) have shown that the rate constant (Ki) for the transfer of tracer from plasma to the irreversible compartment can be calculated from Eq. (8):

$$\frac{\mathrm{ROI}(T)}{Cp(T)} = Ki\,\frac{\int_0^T Cp(t)dt}{Cp(T)} + (Ve + Vp) \tag{8}$$

which is linear for the times $T > t'$ when Ve, the distribution volume of the reversible part (the ratio of the concentration in the reversible compartment to plasma) is constant (for the two-compartment model this is C_1/Cp). An ROI from a study with [^{11}C]L deprenyl-D2 is illustrated in Figure 5a and the irreversible graphical analysis in Figure 5b. L deprenyl is a suicide inhibitor of the enzyme monoamine oxidase B (MAO B) (9). This example can be used to illustrate some of the difficulties involved in analyzing data from irreversibly binding ligands. The process of enzyme inactivation is a multistep process: drug passes into tissue, forms a complex with the enzyme from which an intermediate is produced, ending in a labeled (inactivated) covalently modified enzyme. All the individual rate constants cannot be separately identified since the only measurement other than plasma is the total tissue radioactivity. Enzyme inactivation is therefore represented in terms of the two-compartment model (Figure 6) where k_3 now represents a composite of several steps in the inactivation process. This is generally true of PET models (reversible or irreversible), that is, that the processes are more complex than the models that can be used. In terms of the two-compartment irreversible model, the influx constant Ki can be expressed as seen in Eq. (9):

$$Ki = \frac{K_1 k_3}{k_2 + k_3} = \frac{K_1 \lambda k_3}{K_1 + \lambda k_3} \tag{9}$$

where k_3 is the model parameter associated with the enzyme concentration. We have expressed Ki in terms of two parameters, K_1, which represents the transport of ligand from plasma to tissue, and the combination parameter λk_3, which also contains the ratio of transport constants ($\lambda = K_1/k_2$ mL/mL). Although K_1 and k_2 are functions of blood flow, λ is not. From Eq. (9) it can be seen that Ki depends upon K_1 (blood flow) as well as enzyme concentration (contained in λk_3). Only if $k_2 \gg k_3$, so that $Ki \rightarrow \lambda k_3$, is Ki independent of blood flow. Therefore, to extract a parameter independent of blood flow it is necessary to determine K_1. λk_3 can then be determined from Eq. (9) giving:

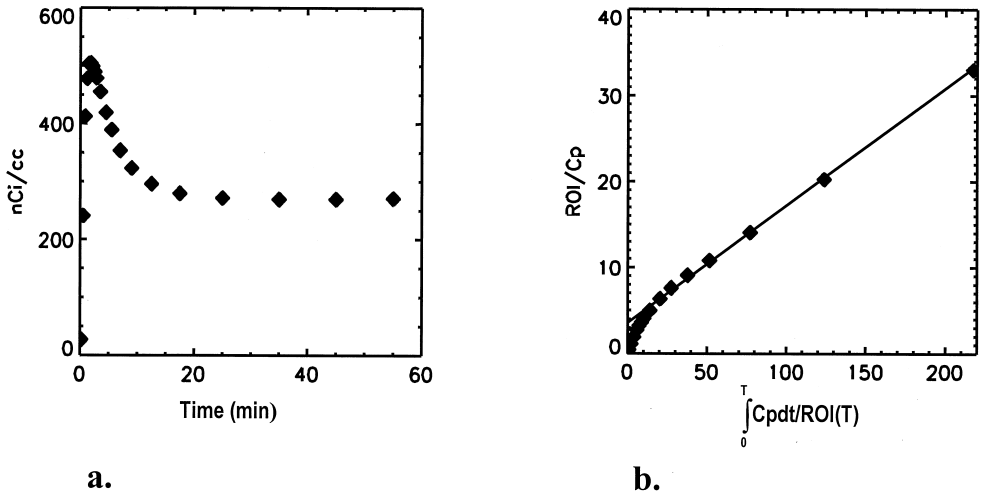

FIG. 5. (a) Regional uptake data from a PET study with [^{11}C]L-deprenyl-D2, an irreversible MAO B inhibitor. (b) Graphical analysis for irreversible ligands, Ki = 0.12 mL min^{-1} mL^{-1} (r = 0.999).

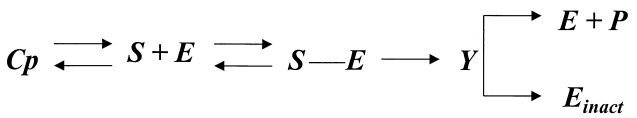

Enzyme inactivation

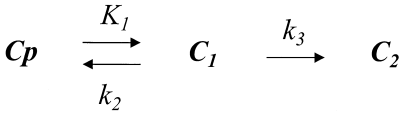

2 Tissue compartment irreversible model

***k_3* is a composite of processes in enzyme inactivation**

FIG. 6. The accepted model for enzyme inactivation and the two-tissue compartment model actually used for describing the binding of L-deprenyl.

$$\lambda k_3 = \frac{K_1 Ki}{K_1 - Ki} \tag{10}$$

A second difficulty encountered in the analysis of data from irreversible ligands is evident in Eq. (10) and that is that K_1 must be sufficiently greater than *Ki* that they can both be determined with some confidence. Otherwise, if $K_1 \sim Ki$, which occurs when the trapping constant k_3 is much greater than K_1 or when $k_2 \ll k_3$, the ligand is said to be flow limited, which means that only one parameter can be determine, K_1, and no information can be obtained about enzyme concentration. Figure 7 illustrates two uptake curves from [^{11}C]L-deprenylH2 and the deuterium-substituted deprenyl, [^{11}C]L-deprenylD2, in the same subject. The difference between K_1 and *Ki* is significantly greater for the D2 compound than for the H2, 0.3, and 0.12 (mL mL^{-1}), respectively. In other regions of interest with higher

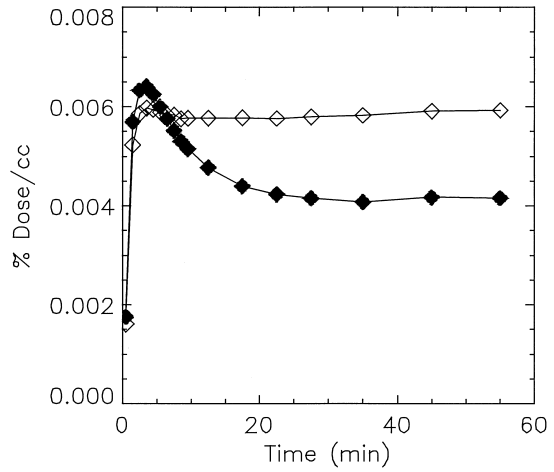

FIG. 7. Regional uptake for [^{11}C]L-deprenyl-H2 (◇) and [^{11}C]L-deprenyl-D2 (◆) in the same individual. K_1 is the same for both [K_1 (H2) = 0.41 mL min^{-1} mL^{-1}, K_1 (D2) = 0.42 mL min^{-1} mL^{-1}]; therefore, the difference is due to the trapping rate (k_3), which is reduced in the D2 compound due to the isotope effect. As a result the *Ki* for D2 is 0.12 mL min^{-1} mL^{-1} and *Ki* for H2 is 0.29 mL min^{-1} mL^{-1}. The sensitivity of the D2 compound to changes in MAO B concentration is much greater than that of deprenyl-H2.

MAO B concentration, the H2 difference was found to be even smaller. The sensitivity of H2 to differences in MAO B concentration is much less than for the D2 ligand. This leads to greater variability in model parameters regardless of the method of estimation. The substitution of deuterium for hydrogen at the reactive site increased the sensitivity by decreasing the rate of trapping. This is an example of the kinetic isotope effect in which the increased mass of the atom involved in the reaction slows the reaction rate (9).

The estimation of K_1 can be made by an iterative nonlinear method using the previously determined *Ki* (when $Ki > 0$) to eliminate one parameter [Eq. (11)]

$$\frac{dC_1}{dt} = K_1 Cp(t) - (k_2 + k_3)C_1 = K_1 Cp(t) - \frac{K_1 k_3}{Ki} C_1$$
$$\frac{dC_2}{dt} = k_3 C_1 \tag{11}$$

The number of parameters to be determined can be further reduced by assuming a value for λ and using Eq. (10) for k_3. This leaves only K_1 to be determined, which can be accomplished in relatively few iterations using only the first part of the uptake curve, which is more sensitive to variations in K_1. In the case of [^{11}C]L-deprenyl, an average estimate of λ could be made from blocking studies (10), although an estimate could also be made from regions with lower concentrations of enzyme (binding sites).

Another alternative is to use a linearized form of the equations [adapted from reference (2)] [Eq. (12)]:

$$\mathrm{ROI}(T) = K_1 \int_0^T Cp(t)\, dt + (k_2 + k_3)\, Z(T)$$
$$Z(T) = Ki \int_0^T \int_0^t Cp(t')\, dt'\, dt - \int_0^T \mathrm{ROI}(t)\, dt \tag{12}$$

where $Z(T)$ can be calculated separately once *Ki* is determined using the method of Patlak. K_1 can then be calculated from a bilinear regression. Only the early time points were used to solve for K_1 ($T < 15$ min). λk_3 calculated by the NLLSQ method (iteratively optimizing all three model parameters) was found to be in good agreement with the value obtained using *Ki* and the linearized equations above for ROI data from test/retest studies with L-deprenyl-D2 (18). It was also found that there was less variability in λk_3 than in k_3 so that the combination parameter like the DV is more reliably estimated than the individual model parameter.

Dhawan *et al.* (5) have found that *Ki* for striatal 6-[18F]fluoro-L-dopa (FDOPA) can be used to separate normals from Parkinson's patients at least as accurately as the model parameter k_3, without the necessity of determining K_1. In the case of FDOPA, K_1 is on the order of 0.05 mL min^{-1} mL as opposed to deprenyl for which K_1 is quite large (~0.5 mL min^{-1} mL^{-1}) and is clearly dominated by blood flow. F or D deprenyl changes in blood flow that occur with age could confound changes in MAO B, if not taken into account. Such considerations depend upon the individual tracer.

Patlak *et al.* (21) have presented a version of the graphical analysis for irreversible ligands that uses a reference region in place of a measured plasma input function. The slope becomes $Ki/(Ve' + Vp')$, where Ve' is the DV of the reference region and Vp' is the blood volume of the reference region.

Wong has used a graphical analysis for the estimation of model parameters for the dopamine D2 ligand [^{11}C]N-methylspiperone

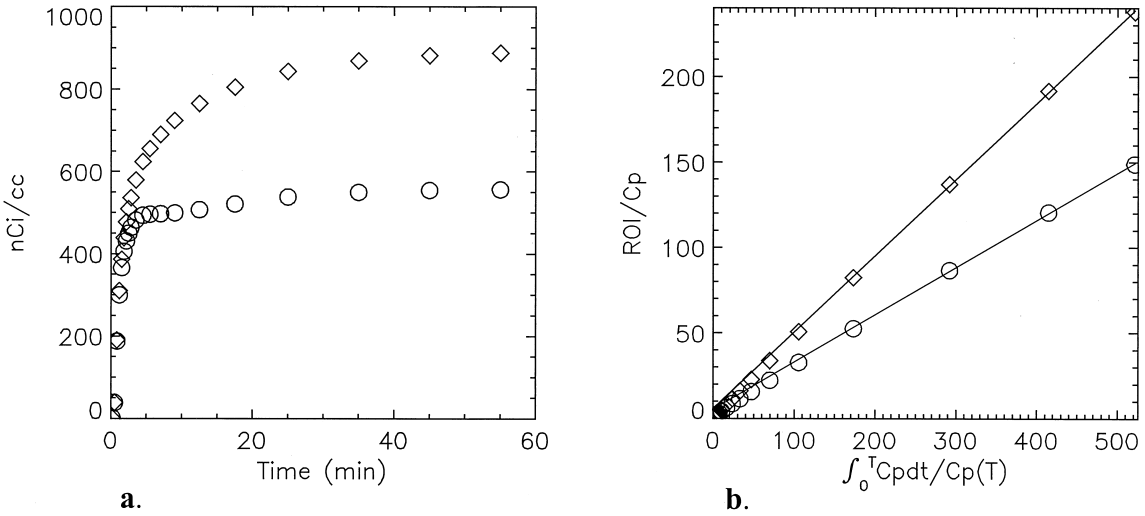

FIG. 8. (a) Data generated from the two-tissue compartment model. Upper curve (◇), DV = 318 mL mL^{-1} with K_1 = 0.5 mL min^{-1} mL^{-1}, k_2 = 0.1, k_3 = 5.0, k_4 = 0.08 (min^{-1}). Lower curve (○), DV = 164 mL mL^{-1} with K_1 = 0.5 mL min^{-1} mL^{-1}, k_2 = 0.125, k_3 = 0.2, k_4 = 0.005 (min^{-1}). (b) Irreversible analyses for the simulated tracer uptake in (a). Ki = 0.28 mL min^{-1} mL^{-1} (◇) and Ki = 0.45 mL min^{-1} mL^{-1} (○).

(NMSP), which appears to bind irreversibly over the period of the experiment. In the case of NMSP there are reference regions such as the cerebellum without specific binding (25, 26). The analysis equation [Eq. (13)]:

$$V(T) = \alpha\theta(T) + \beta(1 - e^{-\theta(T)/\tau}) \tag{13}$$

also uses the normalized time integral of plasma radioactivities [$\Theta = \int_0^T Cp(t)\,dt/Cp(T)$) and the tissue plasma ratio [$V(T)$]. From the reference region, λ is determined, as β when $V(T)$ = REF$(T)/Cp(T)$. The transition of $V(T)$ versus $\Theta(T)$ to a linear phase at later times is determined by τ. The model parameters k_2 and k_3 are determined from α, β, and τ. K_1 was assumed to be the same for both reference region and the region of interest (25). Wong also introduced a ratio index which is the plot of radioactivity in a region of irreversible binding to that in the reference region versus time (as opposed to the normalized time, Θ). This was found to be linear in the case of NMSP (27). Although this is a very simple "graphical" method of analyzing irreversible data, the slope will generally be a function of K_1, except in special circumstances (28).

Data that fall between being clearly reversible or irreversible with respect to the ^{11}C half-life, which limits PET studies to an hour or so, present the greatest difficulty. An example of a tracer with a slow dissociation is illustrated in Figure 8a (open circles) [model parameters K_1 = 0.5 mL min^{-1} mL^{-1}, k_2 = 0.125, k_3 = 0.2, k_4 = 0.005 (min^{-1}), DV = 164 mL mL^{-1}]. The reversible graphical analysis yields an increasing DV, the slope − for 20 to 60 min is 140 and for 30 to 60, 150 (mL mL^{-1}). The irreversible analysis illustrated in Figure 8b gives Ki = 0.28, whereas if k_4 = 0 the value would be 0.31 mL min^{-1} mL^{-1}. In both analyses the composite model parameter associated with the slope is underestimated; however, the irreversible slope (Ki) appears to be the more stable measure. In the second case illustrated in Figure 8a (open diamonds; model parameters K_1 = 0.5 mL min^{-1} mL^{-1}, k_2 = 0.1, k_3 = 0.5, k_4 = 0.08 min^{-1}) the DV is 318 (mL mL^{-1}). The large contribution to the DV comes from k_3 (either from a large binding site concentration or a large rate constant). The irreversible analysis is illustrated in Figure 8b. Although it also appears to give a good linear fit, the value of Ki is 0.45 mL min^{-1} mL, which is very close to that of the K_1. This means that there is almost no information about the receptor/binding site concentration (the flow-limited situation). To know that this is the case, it is necessary to estimate K_1. The reversible analysis gives the correct DV (316 mL mL^{-1}) for times from 18 to 60 min. However, this is simulated data without noise, and DVs of this magnitude would most likely be difficult to estimate accurately from real data.

REMOVING THE BIAS IN PARAMETER ESTIMATES FROM LINEAR METHODS

Although they present an advantage in ease of computation, the linearized equations can introduce a bias in the case of noisy data, since the error term at any given time point contains the error terms at the earlier time points. For example, the linear form of the one-tissue compartment model for scan times ti is [Eq. (14)]:

$$C(t_i) = K_1 \int_0^{t_i} Cp\,dt - k_2 \int_0^{t_i} C_1(t)\,dt + \xi_i \tag{14}$$

with the equation errors, ξ_i, which are not statistically independent (7). This may result in biased parameter estimates. To illustrate this problem, the two-compartment model with parameters given in Figure 9 (uptake illustrated by the solid line) was used to generate 500 data sets with random noise [an example is shown in Fig. 9 (◇)]. The formula used for noise generation (Fig. 9) was chosen so that a greater contribution of noise was included in the shorter earlier scans, which is what is typically observed. The true DV is 12 mL mL^{-1}. From Figure 10 the distribution of DVs determined using the graphical (Fig. 10a) and nonlinear least squares methods (Fig. 10b) are shown. The average DV from the graphical was 11.8 mL mL^{-1} and from the NLLSQ method was 12.05 mL mL^{-1}. Although this is actually a small difference, it does illustrate the trend that the graphical method underestimates the DV in the presence of noise. Furthermore, this underestimate increases as the DV increases (22).

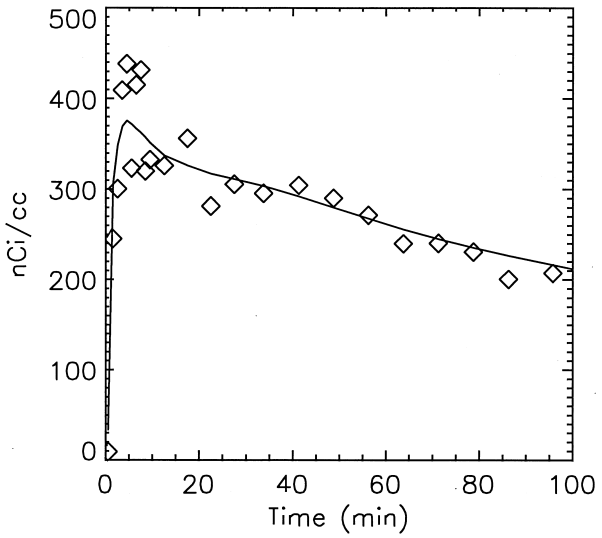

FIG. 9. Data generated from the two-tissue compartment model (DV = 12 mL mL^{-1}) with K_1 = 0.6 mL min^{-1} mL^{-1}, k_2 = 0.2, k_3 = 0.1, k_4 = 0.033 (min^{-1}). The solid line represents the data without random noise [ROI(t)], and the symbols represent data generated with random noise ROI$_N$(t) = ROI(t) + *dev* where *dev* = (0.5 − *xx*)*sc*$\sqrt{}$ROI(t)/Δt, *sc* = 15 (scale factor), and *xx* is a pseudorandom number from 0 to 1. Δt is the scan length.

To overcome the bias problem in the linear solution of compartmental equations, Feng and colleagues (7, 8) introduced a generalized least squares (GLS) method that removes the bias. The one-compartment version of the GLS method is not difficult to implement and provides an iterative method for determining two parameters, K_1 and k_2. An initial estimate of k_2 can be obtained from an analysis of the noisy data either by solution of Eq. (14) or by graphical analysis [−1/intercept from the graphical analysis of Eq. (2) provides an estimate of an effective k_2]. No initial estimate of K_1 is required. Convergence requires only a few iterations.

If the data can be described adequately by a one-tissue compartment model, then this method provides an easy way to estimate the DV without the bias due to noise. It also offers a potential solution for removing the noise in the graphical method. By applying the GLS method for one compartment to the data in two parts (that is, determine one set of parameters for times 0 to t_1 and a second set of parameters for t_1 to the end), the simple one-compartment GLS model can be made to describe data from more complex models, in effect generating a smoothed data set. This is illustrated in Figure 11 for the data of Figure 9. In this case three parameters were used to fit the first part of the curve. The third parameter was a small constant value. The true averaged value is recovered when the graphical analysis is applied to this "smoothed" data (Fig. 10b). The GLS method has also been extended to multicompartment models, which may also be useful in parameter estimation of noisy data (8).

CONCLUSIONS

Graphical methods provide a quick, visual way to obtain information about the kinetics of tracer binding. In some cases these methods can be used without blood sampling if a suitable reference region is available. The reversible analysis requires scanning throughout the study to characterize the tissue uptake curve, which is necessary to evaluate the integral of the uptake. That graphical methods do not require a particular model structure is advantageous, since it is frequently the case that one model does not represent equally well all data sets, thus leading to errors in the model parameter or DV estimates. However, one problem with the linear-type analyses is that they too can introduce a bias into parameter estimates, particularly the reversible analysis for ligands with large DVs. In the case of irreversibly binding ligands, it is in some cases not sufficient to rely on a graphical analysis alone when it is necessary to separate tracer delivery (blood flow) from binding.

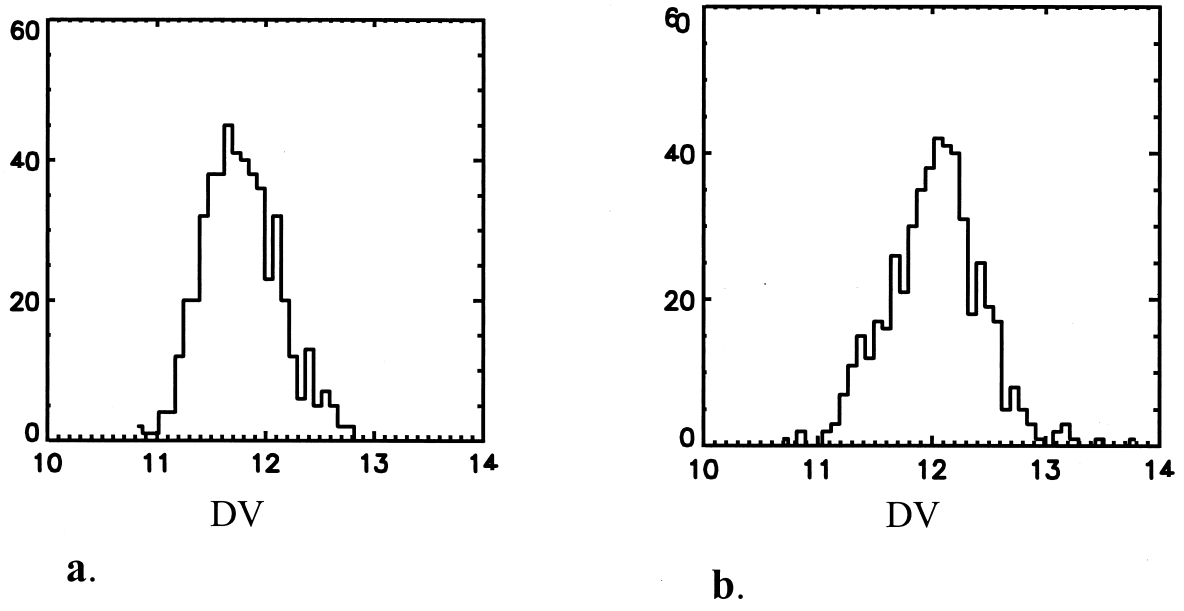

FIG. 10. (a) The distribution of DVs determined using the graphical method from simulated data with random noise (N = 500). (b) The distribution of DVs determined by using the nonlinear least squares method of fitting four parameters to the two-tissue compartment model.

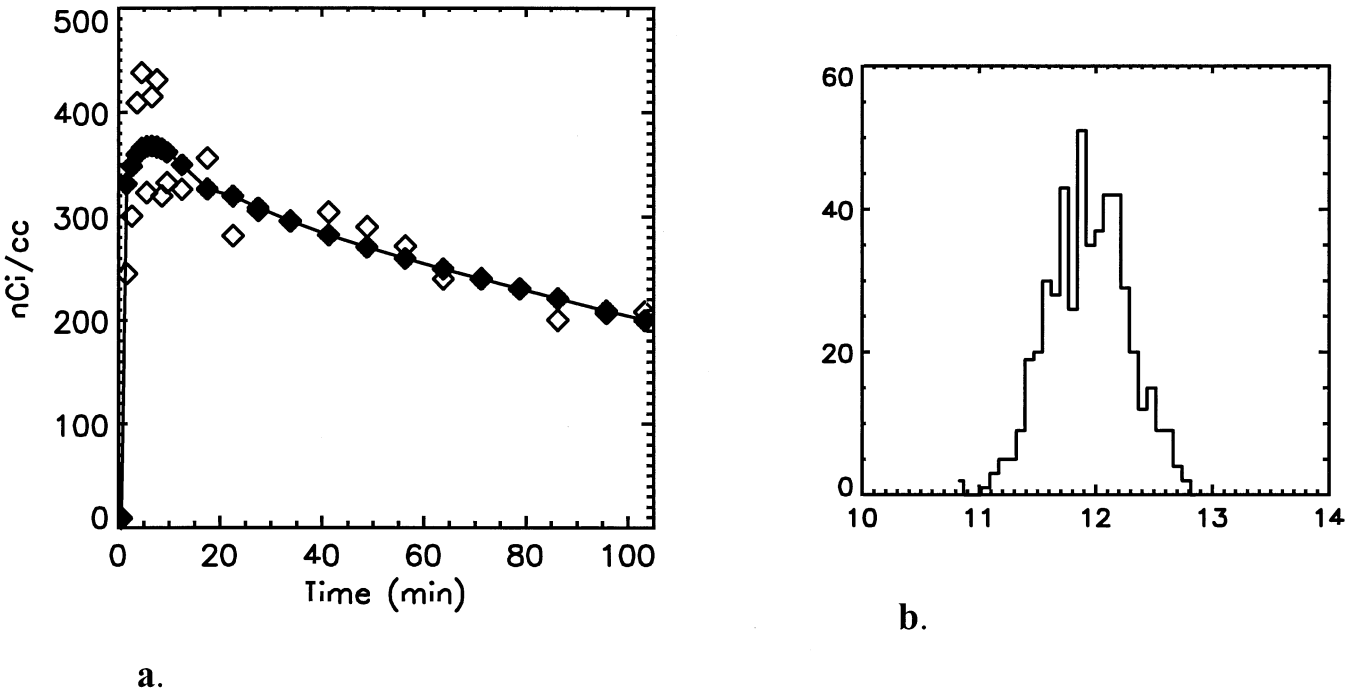

FIG. 11. (a) "Smoothed" data (solid diamonds) generated from a slightly modified version of Feng's GLS method for a one-compartment model. The original data with random noise are indicated by open diamonds. (b) Distribution of DVs from the "smoothed" data set.

However, in these cases the graphical analyses can facilitate the estimation of the important model parameters.

Support was provided by Brookhaven National Laboratory under contract DE-AC02-98CH10886, by the U.S. Department of Energy and its Office of Biological and Environmental Research, and by the National Institutes of Health grant NS15380.

References

1. Blasberg R. G., Patlak C. S. and Fenstermacher J. D. (1979) Measurements of blood-brain transfer constants for three nonmetabolized amino acids. *Int. Soc. Neurochem.* **7:** 238.
2. Blomqvist G. (1984) On the construction of functional maps in positron emission tomography. *J. Cereb. Blood Flow Metab.* **4,** 629–632.
3. Carson R. E., Channing M. A., Blasberg R. G., Dunn B. B., Cohen R. M., Rice K. C. and Herscovitch P. (1993) Comparison of bolus and infusion methods for receptor quantification: Application to [^{18}F]cyclofoxy and positron emission tomography. *J. Cereb. Blood Flow Metab.* **13,** 24–42.
4. Dewey S. L., Smith G. S., Logan J., Brodie J. D., Yu D. W., Ferrierri R. A., King P. T., MacGregor R. R., Martin T. P., Wolf A. P., Volkow N. D., Fowler J. S. and Meller E. (1992) GABAergic inhibition of endogenous dopamine release measured *in vivo* with ^{11}C-raclopride and positron emission tomography. *J. Neuroscience* **12,** 3773–3780.
5. Dhawan V., Ishikawa T., Patlak C., Chaly T., Robeson W., Belakhlef A., Margouleff C., Mandel F. and Eidelberg D. (1996) Combined FDOPA and 3OMFD PET studies in Parkinson's disease. *J. Nucl. Med.* **37,** 209–216.
6. Endres C. J. and Carson R. E. (1998) Assessment of dynamic neurotransmitter changes with bolus or infusion delivery of neuroreceptor ligands. *J. Cereb. Blood Flow Metab.* **18,** 1196–1210.
7. Feng D., Wang Z. Z. and Huang S. C. (1993) A study on statistically reliable and computationally efficient algorithms for the generation of local cerebral blood flow parametric images with positron emission tomography. *IEEE Trans. Med. Imag.* **12,** 182–188.
8. Feng D., Huang S.-C., Wang Z. Z. and Ho D. (1996) An unbiased parametric imaging algorithm for nonuniformly sampled biomedical system parameter estimation. *IEEE Trans. Med. Imag.* **15,** 512–518.
9. Fowler J. S., Wolf A. P., MacGregor R. R., Dewey S. L., Logan J., Schlyer D. J. and Langstrom B. (1988) Mechanistic positron emission tomography studies: Demonstration of a deuterium isotope effect in the monoamine oxidase catalyzed binding of [11C]L-deprenyl in living baboon brain. *J. Neurochem.* **51,** 1524–1534.
10. Fowler J. S., Volkow N. D., Logan J., Schlyer D., MacGregor R. R., Wang G.-J., Wolf A. P., Pappas N., Alexoff D., Shea C., Gatley S. J., Dorflinger E., Yoo K., Kruchowy L. and Fazzini E. (1993) Monoamine oxidase B (MAO B) inhibitor therapy in Parkinson's disease: The degree and reversibility of human brain MAO B inhibition by Ro 19 6327. *Neurology* **43,** 1984–1992.
11. Gjedde A. (1981) High- and low-affinity transport of D-glucose from blood to brain. *J. Neurochem.* **36,** 1463–1471.
12. Ichise M., Ballinger J. R., Golan H., Vines D., Luong A., Tsai S. and Kung H. F. (1995) SPECT imaging of dopamine D2 receptors in humans with iodine 123-IBF: A practical approach to quantification not requiring blood sampling. *J. Nucl. Med.* **36,** 11P.
13. Koeppe R. A., Frey K. A., Kume A., Albin R., Kilbourn M. R. and Kuhl D. E. (1997) Equilibrium versus compartmental analysis for assessment of the vesicular monoamine transporter using (+)-alpha-[11C]dihydrotetrabenazine (DTBZ) and positron emission tomography. *J. Cereb. Blood Flow Metab.* **17,** 919–931.
14. Logan J., Fowler J. S., Volkow N. D., Wolk A. P., Dewey S. L., Schlyer D. J., Macgregor R. R., Hitzmann R., Bendriem B., Gatley S. J. and Christman D. R. (1990) Graphical analysis of reversible radioligand binding from time-activity measurements applied to [N-11C-methyl-(−)-cocaine PET studies in human subjects. *J. Cereb. Blood Flow Metab.* **10,** 740–747.
15. Logan J., Volkow N. D. Fowler J. S., Wang G.-J., Dewey S. L., MacGregor R., Schlyer D., Gatley S. J., Pappas N., King P., Hitzemann R. and Vitkun S. (1994) Effects of blood flow on [11C]raclopride binding in the brain: Model simulations and kinetic analysis of PET data. *J. Cereb. Blood Flow Metab.* **14,** 995–1010.
16. Logan J. (1996) From graphical analysis to multilinear regression analysis of reversible radioligand binding (Letter to the Editor). *J. Cereb. Blood Flow Metab.* **16,** 750–752.
17. Logan J., Fowler J. S., Volkow N. D., Wang G.-J., Ding Y. S. and Alexoff D. L. (1996) Distribution volume ratios without blood sampling from graphical analysis of PET data. *J. Cereb. Blood Flow Metab.* **16,** 834–840.
18. Logan J., Fowler J. S., Volkow N. D., Wang G.-J., MacGregor R. R. and

Shea C. (1999) Reproducibility of repeated measures of deuterium substituted [^{11}C]L-deprenyl([^{11}C]L-deprenyl-D2) binding in the human brain. *Nucl. Med. Biol.* **27,** 43–49.
19. Mintun M. A., Raichle M. E., Kilbourn M. R., Wooten G. F. and Welch M. J. (1984) A quantitative model for the *in vivo* assessment of drug binding sites with positron emission tomography. *Ann. Neurol.* **15,** 217–227.
20. Patlak C., Blasberg R. G. and Fenstermacher J. D. (1983) Graphical evaluation of blood-to-brain transfer constants from multiple-time uptake data. *J. Cereb. Blood Flow Metab.* **3,** 1–7.
21. Patlak C. and Blasberg R. G. (1985) Graphical evaluation of blood-to-brain transfer constants from multiple-time uptake data. Generalizations. *J. Cereb. Blood Flow Metab.* **5,** 584–590.
22. Slifstein M. and Laruelle M. (1999) Statistical bias in the Logan graphical method. *J. Nucl. Med.* **40,** 35P.
23. Volkow N. D., Fowler J. S., Wang G.-J., Dewey S. L., Schlyer D., MacGregor R., Logan J., Alexoff D., Shea C., Hitzemann R., Angrist B. and Wolf A. (1993) Reproducibility of repeated measures of carbon-11-raclopride binding in the human brain. *J. Nucl. Med.* **34,** 609–613.
24. Volkow N. D., Ding Y. S., Fowler J. S., Wang G.-H., Logan J., Gatley S. J., Schlyer D. J. and Pappas N. (1995) A new PET ligand for the dopamine transporter: Studies in the human brain. *J. Nucl. Med.* **36,** 2162–2168.
25. Wong D. F., Gjedde A. and Wagner H. N. Jr. (1986) Quantification of neuroreceptors in the living human brain. I. Irreversible binding of ligands. *J. Cereb. Blood Flow Metab.* **6,** 137–146.
26. Wong D. F., Young D., Wilson P. D., Meltzer C. C. and Gjedde A. (1997) Quantification of neuroreceptors in the living human brain. IV. Effect of aging and elevations of D2-like receptors in schizophrenia and bipolar illness. *J. Cereb. Blood Flow Metab.* **17,** 331–342.
27. Wong D. F., Wagner H. N., Dannals R. F., Links J. M., Frost J. J., Ravert H. T., Wilson A. A. Rosenbaum A. E., Gjedde A., Douglass K. H., Petronis J. D., Folstein J. K., Toung J. K. T., Burns H. D. and Kuhar M. J. (1984) Effects of age on dopamine and serotonic receptors measured by positron emission tomography in the living human brain. *Science* **226,** 1393–1396.
28. Wong D. F., Broussolle E. P., Wand G., Villemagne V., Dannals R. F., Links J. M., Zacur H. A., Harris J., Naidu S., Braestrup C., Wagner H. N. Jr. and Gjedde A. (1988) *In vivo* measurement of dopamine receptors in human brain by positron emission tomography: Age and sex differences. *Ann. NY Acad. Sci.* **515,** 203–214.